BIOCHEMISTRY
including biophysical chemistry & molecular biology

Article

pubs.acs.org/biochemistry

Single-Domain Metallothioneins: Evidence of the Onset of Clustered Metal Binding Domains in Zn-rhMT 1a

Kelly L. Summers,[†,‡] Duncan E. K. Sutherland,[†] and Martin J. Stillman*[,†,‡]

[†]Department of Chemistry, The University of Western Ontario, London, Canada N6A 5B7

[‡]Department of Biology, The University of Western Ontario, London, Canada N6A 5B7

Supporting Information

ABSTRACT: Mammalian metallothioneins bind up to seven Zn^{2+} ions in two distinct domains: an N-terminal β-domain that binds three Zn^{2+} ions and a C-terminal α-domain that binds four Zn^{2+} ions. Domain specificity has been invoked in the metalation mechanism with cluster formation and bridging of the 20 Cys residues taking place prior to saturation with seven Zn^{2+} ions. We report a novel experiment that examines Zn^{2+} metalation by exploiting the expected decrease in K_F at the onset of clustering using electrospray ionization mass spectrometry (ESI-MS). During the titration with Zn^{2+}, the ESI-MS data show that several metalated species coexist until the fully saturated proteins are formed. The relative Zn binding affinities of the seven total sites in the α- and β-fragments were determined through direct competition for added Zn^{2+}. The K_F values for each Zn^{2+} are expected to decrease as a function of the remaining available sites and the onset of clustering. Analysis shows that Zn^{2+} binds to β-rhMT with a greater affinity than α-rhMT. The incremental distribution of Zn^{2+} between the competing fragments and apo-$\beta\alpha$-rhMT (essentially three and four sites competing with seven sites) identifies the exact point at which clustering begins in the full protein. Analysis of the speciation data shows that Zn_5-MT forms before clustering begins. This means that all 20 Cys residues of apo-$\beta\alpha$-rhMT are bound terminally to Zn^{2+} as $[Zn(Cys)_4]^{2-}$ units before clustering begins; there is no domain preference in this first metalation stage. Preferential binding of Zn^{2+} to β- and α-rhMT at the point where $\beta\alpha$-rhMT must form clusters is caused by a significant decrease in the affinity of $\beta\alpha$-rhMT for further Zn^{2+}. The single-domain Zn_5-rhMT, in which there are no exposed cysteine sulfurs, is a key component of the metalation pathway because the lower affinities of the two clustered Zn^{2+} ions allow donation to apoenzymes.

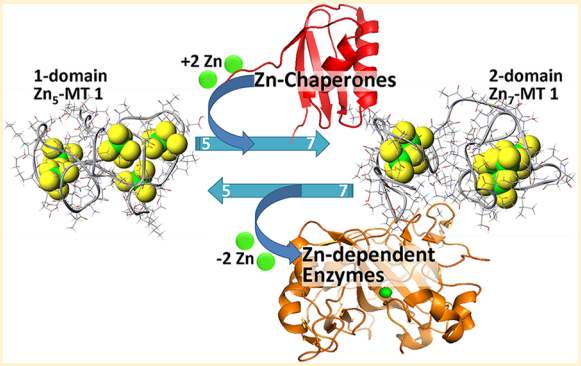

Zinc is a component in proteins, including growth factors, cytokines, receptors, and transcription factors belonging to cellular signaling pathways.[1,2] Zinc thus has a role in a large number of cellular processes.[3] Because zinc is key to so many pathways, levels are tightly regulated. Cellular Zn^{2+} levels are controlled by Zn^{2+} transporters,[4] Zn^{2+} channels,[5] Zn^{2+} sensors,[6] storage proteins like metallothioneins,[7] and metal-response-element-binding transcription factors.[8,9]

When precise levels of Zn^{2+} fail to be maintained, a number of health problems, including growth retardation, immunodeficiency, and neuronal and sensory dysfunctions, result.[9] Because zinc is directly connected to tissue synthesis, severe zinc deficiency in humans can lead to dwarfism. Recently, zinc has been found to reduce the risk of oxidative stress-induced injuries in retinal pigment epithelial cells by inducing and increasing ROS scavenging activities such as MT expression and catalase activity.[10] Thus, understanding the homeostatic control and buffering of cellular Zn^{2+} is vitally important.

At the center of Zn^{2+} homeostatic control is metallothionein (MT). Mammalian MTs are unique small (60−80 residues) metalloproteins with a very high cysteine content (20 residues), and an ability to coordinate multiple metal ions. MTs are found with a Cys-X-Cys homology in organisms from bacteria[11] to fungi[12] to plants and mammals.[13] Of particular significance to this study is the coordination of the essential metal Zn^{2+} to the mammalian protein. Zn_7-MT can be the Zn^{2+} donor for Zn-dependent apoenzymes, for example, *m*-aconitase,[14] carbonic anhydrase,[15,16] and the prototypical transcription factor, Gal4.[17] Removal of Zn^{2+} from the zinc finger-containing transcription factor Sp1 demonstrates that MT also acts as a Zn^{2+} acceptor.[18] ESI-MS studies have also highlighted the stability of partially metalated MT during the transfer of Zn^{2+} from Zn-MT to metal ion chelators or to apoenzymes, which suggests that partially metalated MT may be important in metal ion homeostasis.[19−21]

Key to metal binding in MT are the presence of the 20 Cys SH groups and the absence of cross-linked, oxidized Cys. As a result of this large number of Cys residues, MT also binds strongly to Cd^{2+}, Hg^{2+}, and As^{3+}.[22−24] X-ray diffraction and nuclear magnetic resonance (NMR) studies show that when

Received: January 7, 2013
Revised: March 16, 2013
Published: March 18, 2013

   dx.doi.org/10.1021/bi400021b | *Biochemistry* 2013, 52, 2461−2471

saturated with Zn^{2+} and Cd^{2+}, the metal ions are bound to two distinct metal thiolate clustered binding domains using all 20 Cys residues as both terminal and bridging thiolate ligands. The N-terminal β-domain is capable of binding three Zn^{2+}, three Cd^{2+}, or six Cu^{+} metal ions using nine Cys residues, while the C-terminal α-domain is capable of binding four Zn^{2+}, four Cd^{2+}, or six Cu^{+} metal ions using 11 Cys residues.[25−28]

While the fully metalated proteins have been studied in detail by numerous methods, there are few studies that specifically focus on the metal binding to the apoprotein. ESI-MS data for stepwise As^{3+} binding showed that each As^{3+} ion was bound to three cysteinyl thiolates with no clustering.[22,29,30] Noncooperative metalation has been established for Zn^{2+},[31] Cd^{2+},[32−34] Bi^{3+},[35] and As^{3+}.[22,29,30,36] Two recent papers[37,38] have discussed the binding of zinc to metallothionein and reported binding constants. The study by Namdarghanbari et al.[37] using the zinc sensor FluoZin-3 reported that all the stability constants were approximately 10^{11} and that there was no evidence of a stability constant as low as $\sim 10^{8}$ that had been previously reported by Krezel and Maret.[38]

A description of the metalated state of Zn-MT that accounts for the facility of a fairly simple protein, with unstrained Zn binding sites and with affinities that are nominally greater than those of the recipient Zn-dependent enzymes, to readily donate Zn^{2+} to apoenzymes is lacking in the literature. Consider apometallothionein: it is very flexible, exhibiting very little defined secondary structure.[39] Metalation results in a rigid structure dominated by the metal coordination geometry, which can be digonal, trigonal, tetrahedral, or a combination depending on the metal.[40] As a consequence, "magic numbers" are found for metal binding (the stoichiometric ratios that represent stable saturated clusters), which range from 7 to 18 metal ions per MT protein.[41] Tetrahedral coordination by the Cys thiolates allows seven Zn^{2+} ions to bind using a mixture of terminal and bridging Cys residues and gives a unique three-dimensional structure to Zn_7-MT.

The structure of saturated Zn_7-MT is critical to the donation of Zn^{2+} to apoenzymes. Donation of Zn^{2+} from the saturated protein, with collapse of the clustered binding site structure, would lead to subsequent exposure of Cys thiols to the cellular environment. Oxidation would rapidly result.[14,15,17,42] The conundrum is thus how the Zn^{2+} ions bound in MT transfer to apoenzymes with lower binding affinities without destroying the MT that still has six Zn^{2+} ions bound and why such a disastrous consequence would be a property of MT.

In this paper, we propose that the donated zincs come from the clustered binding sites, but following donation, a terminally bound zinc structure forms, which means that no thiols are exposed to oxidation. Our results show that the initial metalation of MT does not occur in a domain specific manner; rather, the 20 Cys residues allow up to five Zn^{2+} ions to bind terminally to the thiolates in a "beaded necklace"-like fashion. Subsequent metalation to Zn_6- and Zn_7-$\beta\alpha$-rhMT 1a requires a complete structural rearrangement, loss of the single-domain structure, and formation of the clustered domains. Clustering takes place via bridging interactions with, most importantly, a concomitant reduction in K_F for those two last sites. Affinity-driven selectivity in binding is the hallmark of the cellular buffering of Zn^{2+}, and the presence of two Zn^{2+} ions in weaker binding sites facilitates this effect. The loss of Zn^{2+} through equilibrium-driven transfers reverses this process, re-forming the protected Zn_5-Cys_{20} structure.

EXPERIMENTAL PROCEDURES

Protein Preparation. The expression and purification methods used to purify human recombinant MT isoform 1a have been previously reported.[43] β-rhMT, α-rhMT, and $\beta\alpha$-rhMT 1a proteins used in this study were based on the following 38-residue, 41-residue, and 72-residue sequences, respectively: MGKAAAACSC ATGGSCTCTG SCKCKECKCN SCKKAAAA, MGKAAAAC CSCCPMSCAK CAQGCVCKGA SEKCSCCKKA AAA, and MGKAAAACSC ATGGSCTCTG SCKCKECKCN SCKKAAAACC SCCPMSCAKC AQGCVCKGAS EKCSCCKKAA AA. There are 9, 11, and 20 Cys residues present in β-, α-, and $\beta\alpha$-rhMT, respectively, and no disulfide bonds. The sequence of this recombinant MT 1a contains a quadruple-alanine insert at both termini of the peptide domains, as well as the N-terminal and linker region of the full protein. NMR, CD, and UV absorption studies have shown no perturbation as a result, when compared with native human MT 1a.[44] The expression system included, for stability purposes, an N-terminal S-tag (MKETAAAKFE RQHMDSPDLG TLVPRGS). Recombinant proteins were expressed in *Escherichia coli* BL21(DE3). All cell lines were transformed using the pET29a plasmid. The S-tag was removed using a Thrombin CleanCleave Kit (Sigma). Rigorous evacuation followed by argon saturation was used to impede oxidation of the cysteine residues. Concentrated HCl was used to demetalate protein samples, followed by desalting on a G-25 (Sephadex) column. Unless specifically stated otherwise, all data discussed in this paper are from the same, recombinant, human MT isoform 1a with the specific sequence shown above.

ESI-MS Procedures. Protein solutions were prepared in dilute formic acid in deionized water (pH 2.7). The pH values of final ESI-MS solutions were adjusted using concentrated NH_4OH. Protein concentrations were determined by remetalation of a portion of the sample with Cd^{2+} ions, and Cd-rhMT was monitored by UV absorption spectroscopy using the absorbance at 250 nm, which corresponds to the ligand-to-metal charge transfer transition generated by cadmium-bound MT ($\varepsilon_{\beta 250}$ = 36000 M^{-1} cm^{-1}; $\varepsilon_{\alpha 250}$ = 45000 M^{-1} cm^{-1}; $\varepsilon_{\beta\alpha 250}$ = 89000 M^{-1} cm^{-1}). $ZnSO_4$ was prepared in deionized water; all molar equivalents were determined using atomic absorption spectrometry.

ESI-MS data were collected on an electrospray ionization time-of-flight (ESI-TOF) mass spectrometer (micOTOF-II, Bruker Daltonics, Toronto, ON) in the positive ion mode. NaI was used as the calibrant. Spectra were deconvoluted using the Bruker Compass DataAnalysis software package.

Molecular Modeling. MM3 and MD calculations, parametrized using the modified force field described by Chan et al. and using the dielectric constant for water (78.4), were conducted to obtain the minimum-energy structure of apo-$\beta\alpha$-rhMT 1a to Zn_7-$\beta\alpha$-rhMT 1a.[45] All MM3 and MD calculations and model structure rendering were conducted using Scigress version 3.0 (Fujitsu Poland). The original Cd_7-$\beta\alpha$-rhMT 1a was modified to produce molecular models for Zn_5-$\beta\alpha$-rhMT 1a.[43] The structure was energy minimized using the MM3 calculation followed by the MD simulation at 300 K for 5000 ps.

RESULTS AND DISCUSSION

The experiments reported here provide insight into the role of metallothioneins in zinc homeostasis by showing that there is a wide range of binding constants for the seven bound Zn^{2+} ions.

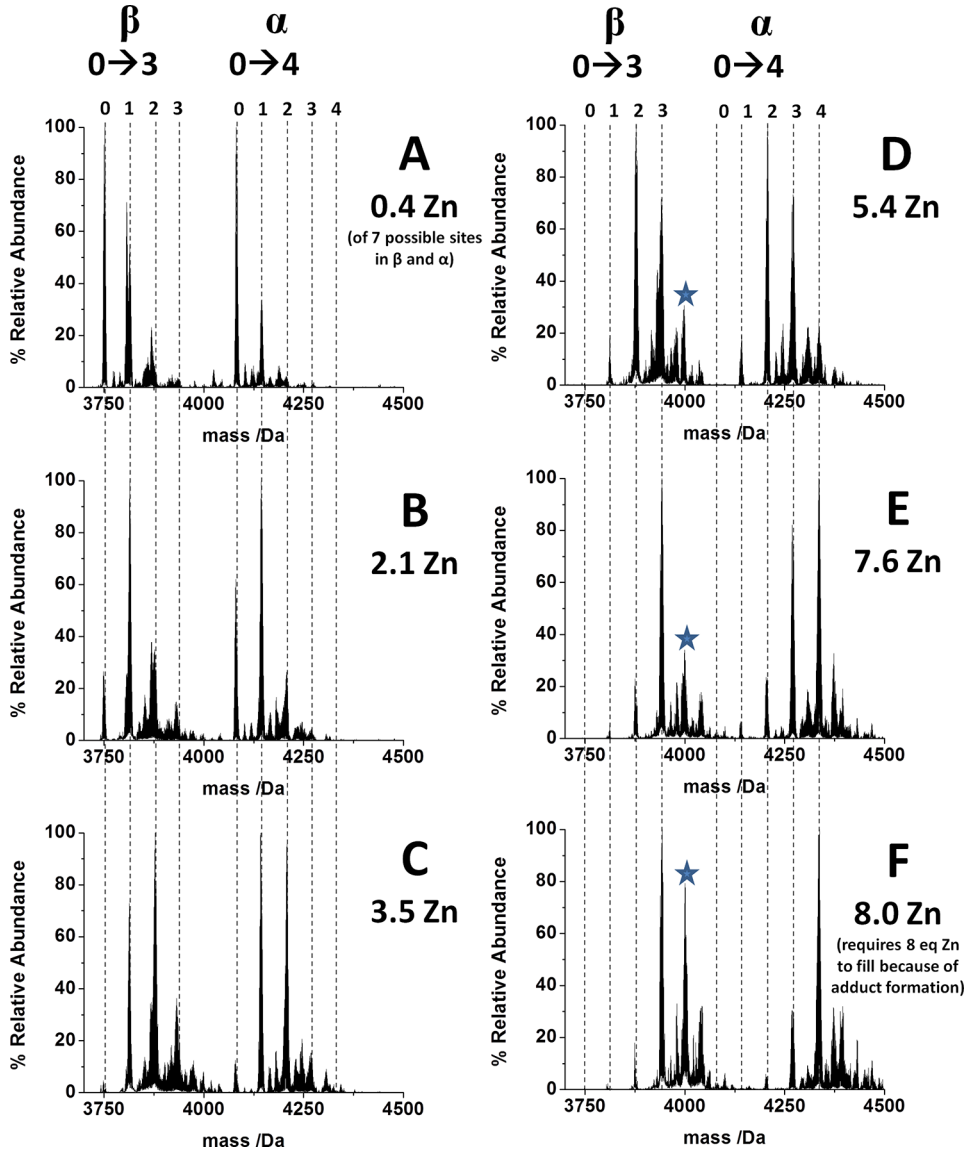

Figure 1. ESI deconvoluted mass spectra recorded during the competitive titration of apo-β- and apo-α-rhMT, each at 29.2 μM at pH 9.2, with $ZnSO_4$. Aliquots of Zn^{2+} (8.3 mM) were added to the protein solution on ice (0.4, 2.1, 3.5, 5.4, 7.6, and 8.0 equiv). Dotted lines follow metal binding. The most intense species for both the β- and α-domain have been normalized to 100% relative abundance. An asterisk indicates the presence of Zn adducts. The raw m/z data can be found in Figure S1 of the Supporting Information.

These data also explain how donation of Zn^{2+} to apoenzymes does not result in the unraveling of binding sites and exposure of Cys to oxidation and how metal reception and donation allow for the equilibrium-driven transfer of Zn^{2+} into and out of MT.

ESI-MS data were recorded for the incremental addition of Zn^{2+} to solutions in which the isolated domains and the two-domain rhMT 1a competed for Zn^{2+}. Although the Zn binding sites in these three proteins would be expected to exhibit the same K_F values, there are systematic differences. The competition experiment exploits the differences in K_F introduced by the change from terminal binding in $Zn_5(Cys)_{20}$ to clustered binding in $Zn_7(Cys)_{20}$. These results provide insight into the role of MTs in zinc homeostasis because this range of K_F values provides a buffering capacity that extends over a range of zinc concentrations.

Metal binding in MT has been studied in a number of metalation, demetalation, and metal replacement experiments conducted under equilibrium and kinetic conditions.[41,46] Previous metalation experiments, such as copper luminescence,[28,47] provide only an averaged measure of metalation, not the exact speciation over all sites. The discriminating capacity of ESI-MS provides simultaneous information about all species present and their respective dynamic metalation states. Because binding of Zn^{2+} to MT is noncooperative,[31,48] the exact distribution at each step in the titration can be determined. There may be some ambiguity in the exact speciation of the intermediate products arising from metalation and demetalation when they are studied by ESI-MS because the thermodynamic structures of the apoprotein for metalation and the fully metalated protein for demetalation are clearly not the same.[49−51]

Competitive Metalation of β- and α-rhMT 1a with Zn^{2+}. Figure 1 shows the mass spectra recorded during the competition experiment in which incrementally added Zn^{2+} is distributed between the β-domain (with three potential sites)

dx.doi.org/10.1021/bi400021b | *Biochemistry* 2013, 52, 2461−2471

and the α-domain (with four potential sites). The domains are present in equal concentrations in the solution. There is a slight Zn^{2+} contaminant, ~0.4 equiv of total protein. The Zn^{2+} equivalents added to the solution are relative to the total protein concentration (β-domain + α-domain = 7 binding sites). The charge state data are shown in Figure S1 of the Supporting Information.

The deconvoluted data (Figure 1) fall into two distinct sets reflecting the different masses of the β- and α-fragments. The experimental data show the domain preference for each added Zn^{2+} (Figure 1). Because there are seven binding constants in total, Zn^{2+} binding will be directed by the largest K_F. Changes are observed in the fractional distribution of Zn^{2+} between the two domains as the level of Zn loading increases. Figure 2

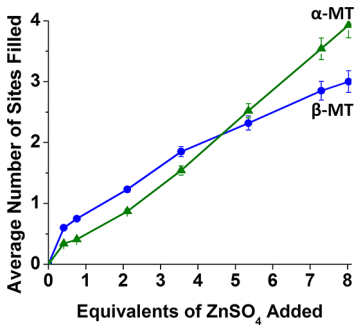

Figure 2. Average metalation of the β-domain (blue) and α-domain (green) as a function of addition of Zn^{2+} to a solution containing both in equal concentrations. The data were calculated from the spectra shown in Figure 1.

shows the average metalation of the fragments based on the data in Figure 1. Between zero and approximately five Zn^{2+} ions added, the β-domain binds a greater fraction of the Zn^{2+}. After approximately five Zn^{2+} ions, the α-domain binds a greater fraction because it still has two sites available. These ESI-MS data are significant because one would intuitively predict that (i) either both domains would bind the added Zn^{2+} equally or (ii) the α-domain might bind a greater fraction because of the four available sites versus the three available sites in β-rhMT. However, the β-domain clearly binds a greater fraction of the available Zn^{2+} up to $Zn_2\beta$-rhMT. The crossover when the β-domain has bound two Zn^{2+} ions may be interpreted as a statistical advantage of the third and fourth sites in the α-domain.[22]

Modeling the competition experiment is an important feature of this study because it allows the proposed mechanism to be tested. Figure 3 shows the experimental Zn^{2+} speciation data following Zn^{2+} metalation of apo-β-rhMT (A) and apo-α-rhMT (C), in a solution that contains both. The simulation, split into two parts to show the relative Zn^{2+} binding for each domain (B and D), uses seven diminishing K_F values to represent the seven total sites in the β- and α-domains. The K_F values were determined from the three-way competition experiment involving the two domains and the full protein (Figure 4). It is striking that the model strongly mirrors the experimental data, confirming our interpretation that the domains compete for Zn^{2+} with the β-domain initially binding and being preferred over the α-domain.

Competitive Metalation of the Isolated β- and α-Domains and the Full, Two-Domain $\beta\alpha$-rhMT 1a. When all three species (β-, α-, and $\beta\alpha$-rhMT) are mixed, they compete for added Zn^{2+} with a total of 14 binding sites but with different, although clearly very similar, K_F values.

Figure 4 shows the experimental ESI-MS data for the case in which apo-β- and apo-α-rhMT are mixed with the full apo-$\beta\alpha$-protein and Zn^{2+} is added incrementally. The raw MS data (Figure S2 of the Supporting Information) are complicated because the charge states for the two fragments and the full protein for each metalated state are superimposed. The deconvolution data (Figure 4) allow additional information to be extracted: (i) the proportion of Zn^{2+} captured by each protein while in equilibrium with the other two species up to full saturation of all three proteins (Figure 5) and (ii) the average metal loading of each species as a function of added Zn^{2+} during competition (Figure 6).

The experimental data in Figure 4 show that $\beta\alpha$-rhMT dominates Zn^{2+} binding up to ~6.4 Zn^{2+} ions added (C). This is clear from the comparison of Zn species in panels A, C, and E of Figure 5, where Zn_3- and Zn_4-$\beta\alpha$-rhMT have formed, but only Zn_1 and Zn_2 have formed in the isolated domains. If the binding constants were equal, the Zn^{2+} would be distributed evenly among the three proteins. The Zn^{2+} speciation shown in panels A, C, and E of Figure 5 immediately and unambiguously shows that the K_F values for the first four Zn^{2+} ions in $\beta\alpha$-rhMT must be greater than comparable K_F values in the two isolated domains because when the β-rhMT and α-rhMT bind two Zn^{2+} ions, the full $\beta\alpha$-rhMT protein has bound four Zn^{2+} ions.

Panels B, D, and F of Figure 5 show the simulation of the stepwise distribution of Zn^{2+} in the 14 sites when all three proteins are mixed. The simulation very closely models the experimental data. The K_F values required in the model illustrate the experimental distribution showing that $\beta\alpha$-rhMT will bind Zn^{2+} preferentially into sites 1−4. Because all sites are in equilibrium, there is a distribution between available sites, not a domain specific mechanism.

The data show that the first four $\beta\alpha$-rhMT binding sites have a higher binding constant than the isolated domains. This is initially unexpected as the binding sites, at this stage of the metalation, comprise terminally bound Zn^{2+}, in $Zn(Cys)_4$ units, which would be expected to exhibit almost identical K_F values for proteins as similar as these three species. The analysis of the As^{3+} binding kinetics by Ngu et al. predicted this effect.[22,29,30] Because there are more available sites in $\beta\alpha$-rhMT than in the isolated domains, the K_F values of the first four sites of $\beta\alpha$-rhMT dominate. The analysis indicates the first four Zn^{2+} ions bind to $\beta\alpha$-rhMT preferentially because of the statistical effect of seven sites (more than four in α and more than three in β). However, the statistical model does not account for the greatly reduced K_F for the sixth and seventh Zn^{2+} sites. We will interpret this change in K_F after describing Figure 6.

Speciation during Zn^{2+} Metalation of the Domains. Panels A and B of Figure 6 provide the average metalation data for the competition experiment in which the full MT protein and the isolated fragments compete for the same Zn^{2+} (calculated from data in Figure 5A,C,E).

Figure 6 is a complicated summary of data that describe the buffering and Zn donating properties of MT. There are three main features of the data shown in panels A and B. (i) In the presence of $\beta\alpha$-rhMT, the β-domain still binds Zn^{2+} preferentially to the α-domain up to the Zn2 point. The two traces for α- and β-rhMT in competition with $\beta\alpha$-rhMT (Figure 6A) are almost identical to the traces shown for α-rhMT and β-rhMT in competition with each other (Figure 2). The similarity in the trend of the speciation illustrates that the respective K_F

dx.doi.org/10.1021/bi400021b | Biochemistry 2013, 52, 2461−2471

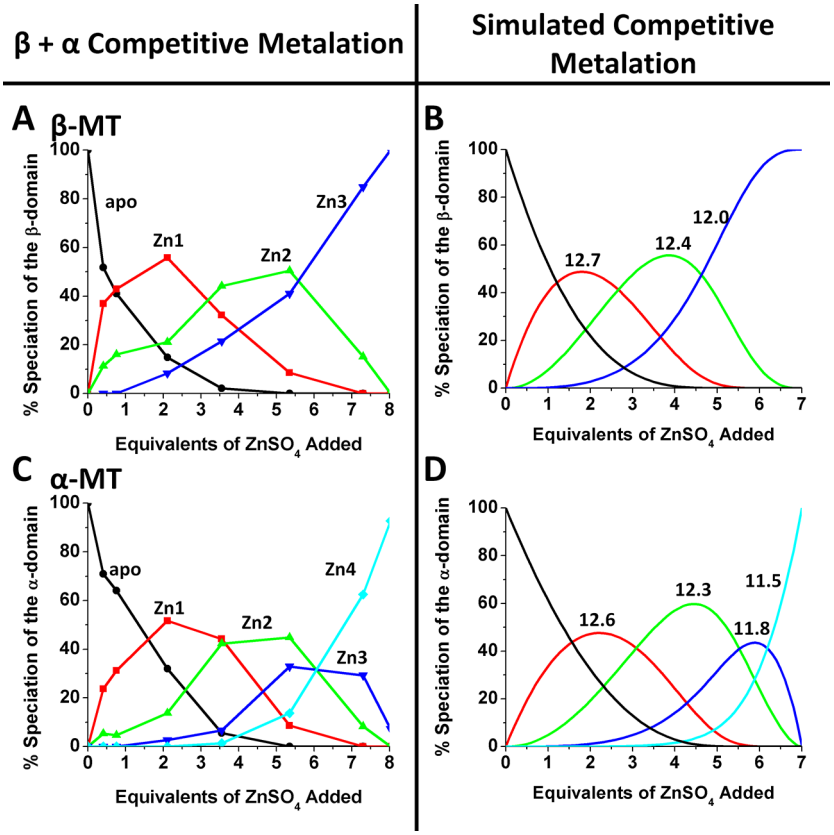

Figure 3. Stepwise simultaneous metalation of apo-β-rhMT (A) and apo-α-rhMT (C) under competitive conditions, using Zn^{2+} to form Zn_n, where n corresponds to the number of metals bound to each protein. Simulation of the metalation of β-rhMT (B) and α-rhMT (D) with $\log_{10}(K_F)$ values for the α-domain of 12.6, 12.3, 11.8, and 11.5 and for the β-domain of 12.7, 12.4, and 12.0. Each line corresponds to a different metalation state: Zn_0 (black), Zn_1 (red), Zn_2 (green), Zn_3 (blue), and Zn_4 (cyan).

values are very similar. Clearly, this illustrates that the K_F values are constants for the addition of Zn^{2+} to the fragments irrespective of whether they are in the presence of $\beta\alpha$-rhMT. The simulations confirm that the K_F values are reliable and account for the experimental data in two separate types of competition experiments. (ii) The presence of $\beta\alpha$-rhMT reduces the overall Zn loading of the isolated domains compared with the Zn loading in the absence of $\beta\alpha$-rhMT (Figure 2). This is an important effect because it means that the isolated domains are binding proportionally less Zn^{2+}. This is a buffering property that results from the equilibrium among all three species. (iii) $\beta\alpha$-rhMT dominates Zn binding until the eighth Zn^{2+} is added to the solution.

In Figure 6B, the average number of Zn sites filled for $\beta\alpha$-rhMT is compared with the sum of the Zn sites filled in the isolated β- and α-domains. If the K_F values were the same for each Zn^{2+} site (i.e., the Zn1 site in $\beta\alpha$, β, and α), then the two lines should be coincident. Clearly, $\beta\alpha$-rhMT preferentially binds more Zn^{2+} into its sites compared with the same total number of sites in the isolated domains (i.e., β- plus α-rhMT), but only until the eighth Zn^{2+} is added. After that, the isolated domains preferentially bind more Zn^{2+} even though the same number of sites is available.

Figure 6C shows the results of a simulation in which the stepwise distribution of Zn^{2+} was calculated on the basis of the K_F values shown in Figure 5. Again the simulated data match the experimental data (A and B) almost exactly, confirming the model that considers diminishing K_F values for all sites and the statistical advantage of the seven sites in $\beta\alpha$-rhMT over the four plus three sites in the isolated domains. The five key features (marked a′−e′) on the lines in panels A and B are reproduced exactly in the simulation in panel C (marked a−e, respectively), confirming the reliability of the K_F values used in the simulation. The letters a′ and a indicate the regions where binding of Zn^{2+} to β-rhMT is preferred over that to α-rhMT, while the letters b′ and b indicate the crossover point after which binding of Zn^{2+} to α-rhMT is preferred over that to β-rhMT. In panels B and C of Figure 6, the letters c′ and c indicate where binding of Zn^{2+} to $\beta\alpha$-rhMT is preferred over that to the sum of the Zn^{2+} binding sites (three plus four) in the two isolated fragments. This initial preference for binding of Zn^{2+} to the seven available sites of the full, two-domain protein (c′) is critically important to this study, and it is a major result that this property is reproduced closely in the simulation shown in Figure 6C, which is based on all 14 K_F values. Subsequently, as the Zn^{2+} concentration was increased in a stepwise fashion, the Zn^{2+} binding preferences became equal and the Zn loading of the full, two-domain protein equaled that of the sum of the isolated fragments. In panels B and C of Figure 6, the letters d′ and d identify the crossover point following which binding of Zn^{2+} by the combined isolated fragments is preferred (e′). Overall, the simulation in Figure 6C reproduces each of the key features of the experimental data (a−e).

Cluster Formation: A Greater Reduction in K_F for $\beta\alpha$-rhMT 1a at the Zn6 Point. The point at which the isolated domains begin to preferentially bind more Zn^{2+} is that at which the sixth Zn^{2+} binds to $\beta\alpha$-rhMT. Structurally, this is where the $\beta\alpha$-protein must use bridging Cys residues for the $Zn_6(Cys)_{20}$

dx.doi.org/10.1021/bi400021b | *Biochemistry* 2013, 52, 2461−2471

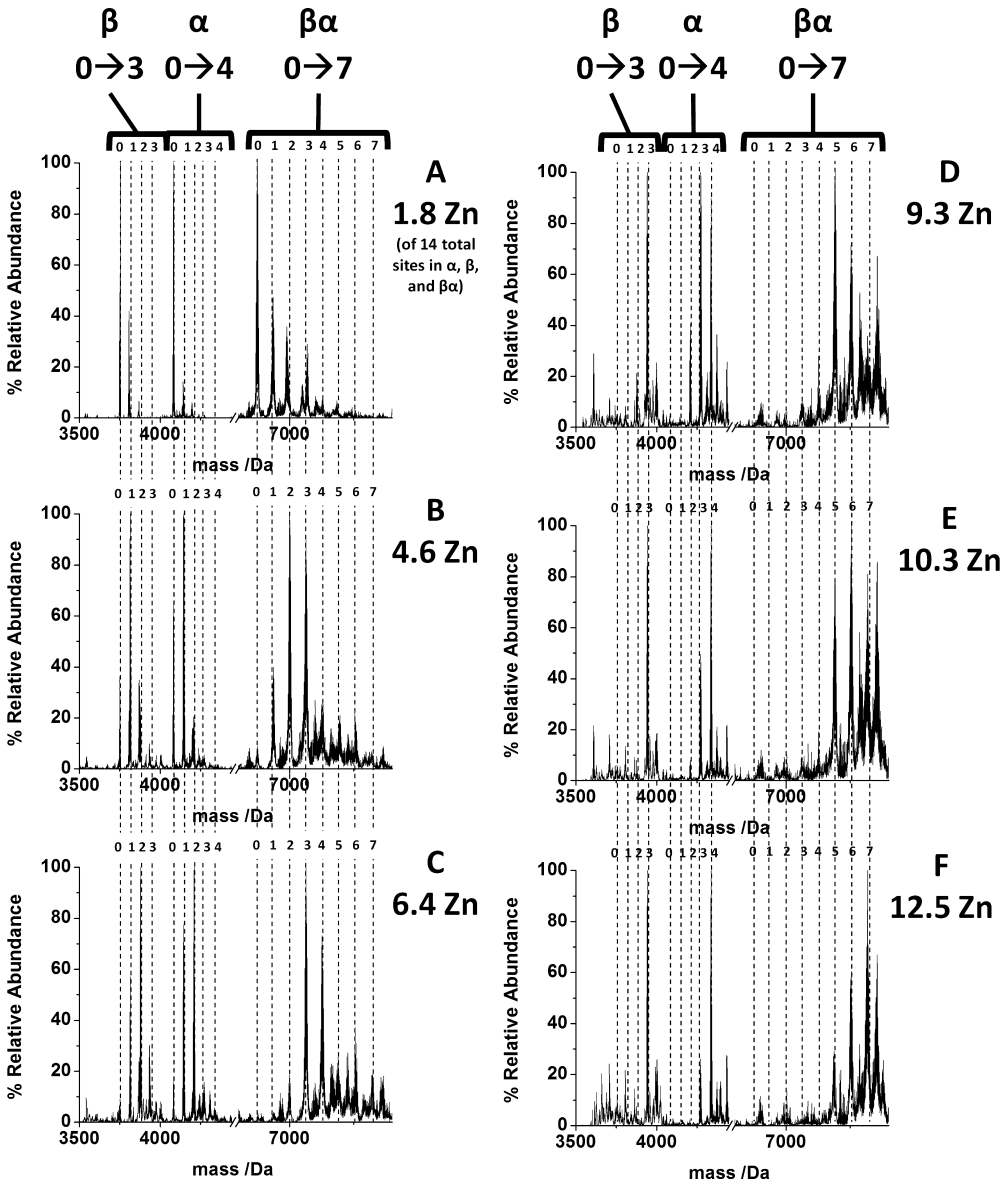

Figure 4. ESI deconvoluted mass spectra for the competitive titration of a solution containing equimolar concentrations (29.9 μM each) of apo-β-, apo-α-, and apo-$\beta\alpha$-rhMT with $ZnSO_4$ at pH 7.8. Aliquots of Zn^{2+} (7.3 mM) were added to the protein (based on 14 available sites) as 1.8, 4.6, 6.4, 9.3, 10.3, and 12.5 equiv. Dotted lines follow metal binding. The most intense species for β-, α-, and $\beta\alpha$-rhMT have been normalized to 100% relative abundance. The titration stopped prior to 14 equiv because of the increased noise from the high $ZnSO_4$ concentration. The raw m/z data are shown in Figure S2 of the Supporting Information.

structure compared with the string of five isolated, terminally coordinated $Zn(Cys)_4$ sites. The simulation in Figure 5 shows that the K_F values for both Zn6 and Zn7 are smaller than the K_F values of α-rhMT's Zn4 and β-rhMT's Zn3, so the isolated domains preferentially bind the incoming Zn^{2+}.

These data show that $\beta\alpha$-rhMT exhibits higher K_F values relative to those of the isolated domains for the first five Zn^{2+} ions. Following the statistical advantage of the seven available sites versus the three sites of β-rhMT and the four sites of α-rhMT, the K_F values of all three proteins are balanced and approximately equal once the fifth Zn^{2+} binds to $\beta\alpha$-rhMT (Figures 5B,D,E and 6). After this point, the domains metalate at the expense of the full protein because cluster formation in the isolated domains is not as disruptive and the K_F values are not as diminished.

This interpretation of the change in K_F values for the sixth and seventh Zn^{2+} ions in Zn_n-$\beta\alpha$-rhMT (n = 6 or 7) is based on the properties of Cys ligands. The onset of bridging Cys in the $\beta\alpha$-protein led to a significant decrease in K_F for each step after five Zn^{2+} ions had terminally bound to all 20 Cys residues. The data suggest that it is the sixth Zn^{2+}, with a decreased affinity for MT relative to the isolated domains, that causes bridging to occur and forces the two-domain structure to form. The model (Figure 7) suggests massive rearrangements are necessary to change the structure from the five-$Zn(Cys)_4$ beaded-necklace structure to the clustered domain-separated $Zn_7(Cys)_{20}$ structure. The seventh Zn^{2+} completes the two-domain structure, leading to the two well-known, saturated binding domains: Zn_4Cys_{11} and Zn_3Cys_9.

In summary

$$apo(Cys)_{20}\beta\alpha\text{-rhMT} + 5Zn^{2+} \rightarrow (Zn(Cys)_4)_5\beta\alpha\text{-rhMT}$$

dx.doi.org/10.1021/bi400021b | *Biochemistry* 2013, 52, 2461−2471

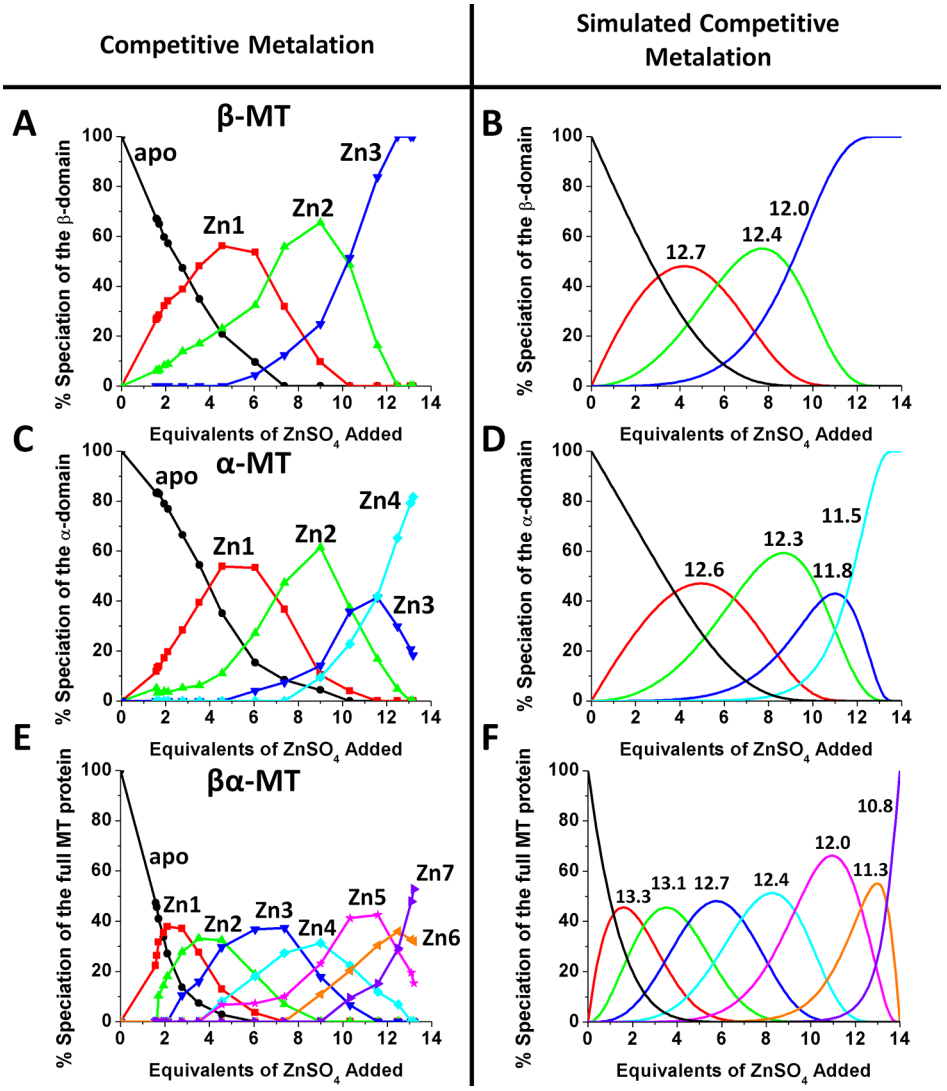

Figure 5. Stepwise, simultaneous metalation of apo-β-rhMT (A), apo-α-rhMT (C), and apo-$\beta\alpha$-rhMT (E), under competitive conditions using Zn^{2+} to form Zn_n, where n corresponds to the number of metals bound to each protein. Simulation of the metalation of the isolated domains (B and D) and the full MT protein (F) using $\log_{10}(K_F)$ values for the α-domain of 12.6, 12.3, 11.8, and 11.5, for the β-domain of 12.7, 12.4, and 12.0, and for the full MT protein of 13.3, 13.1, 12.7, 12.4, 12.0, 11.3, and 10.8. Each line corresponds to a different metalation state: Zn_0 (black), Zn_1 (red), Zn_2 (green), Zn_3 (blue), Zn_4 (cyan), Zn_5 (magenta), Zn_6 (orange), and Zn_7 (purple).

$$(Zn(Cys)_4)_5\beta\alpha\text{-rhMT} + 2Zn^{2+} \rightarrow (Zn_3Cys_9)(Zn_4Cys_{11})\beta\alpha\text{-rhMT}$$

Relevance of the As^{3+} Binding Kinetics Study. Previous metal binding studies of rhMT with As^{3+} demonstrated that the metal binding affinity of MT is directly dependent on the number of available binding sites. It is important at this point to recall that As^{3+} binds to the 20-Cys MT using only terminal Cys so that saturation occurs with six As^{3+} ions binding using three Cys residues per As^{3+} with no bridged Cys. The K_F for each metal bound essentially decreased statistically from the first As^{3+} bound to the sixth As^{3+} bound of the saturated As_6-$\beta\alpha$-rhMT.[22,29,30,36] Significantly, a similar trend is observed with Zn^{2+} binding (Figure 5).

These results are critical in placing Zn-MT between the Zn sensors that must be present in mammalian cells, which may be similar to the ZiaR[52] and Zur[53] sensors in microorganisms. The cellular Zn sequestration equilibrium shows that (i) the K_F values are directly proportional to the number of available binding sites, (ii) there is no domain preference for Zn^{2+} until terminal thiolates bridge at Zn6 and then Zn7, (iii) bridging interactions lead to a significant decrease in the observed K_F values, and (iv) donation of Zn6 and Zn7 to apoenzymes will not expose any of MT's 20 Cys residues to oxidation, allowing subsequent acquisition and donation. Clearly, in vivo the redox situation will be more complicated, involving the reducing effects of glutathione. In effect, the sixth and seventh Zn^{2+} ions act as the buffer-active Zn^{2+}, with K_F values lower than those of the five structural Zn^{2+} ions.

From our results, we can see that the proposal by Ngu et al. is followed up to Zn4 and Zn5.[22,29,30,36] The significant difference between the two metal ion species is that Zn_7-rhMT requires bridging Cys, while bridging cannot occur during As^{3+} metalation, leading to As_6-MT as the saturated species. Therefore, the key species in Zn^{2+} metalation is Zn_5-$\beta\alpha$-rhMT, which represents an "islet of stability" where the K_F for the conversion of Zn_5-$\beta\alpha$-rhMT to Zn_6-$\beta\alpha$-rhMT is sufficiently low to allow near quantitative formation of the Zn_5 species.

dx.doi.org/10.1021/bi400021b | Biochemistry 2013, 52, 2461−2471

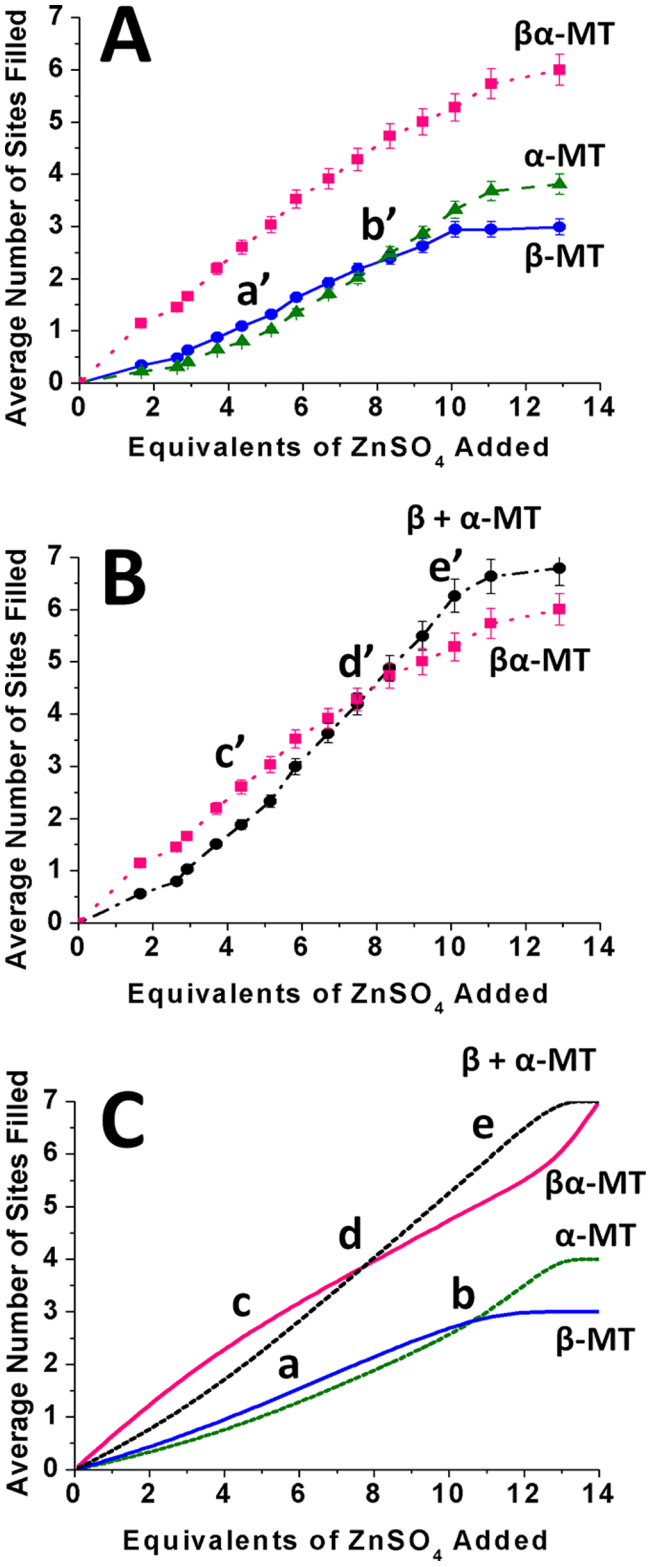

Figure 6. Experimental and simulated metalation states of apo-β-rhMT, apo-α-rhMT, and apo-$\beta\alpha$-rhMT when metalated with Zn^{2+} under competitive conditions. (A) Average number of Zn^{2+} ions bound in the β-domain (blue), the α-domain (green), and the full MT protein (red) (based on data in Figure 5). (B) Comparison of the average metalated states of the sum of the two domains (●) and the full protein as a function of added Zn^{2+}. (C) Simulation of the stepwise distribution of Zn^{2+} among the three protein species using the $\log_{10}(K_F)$ values of 12.6, 12.3, 11.8, and 11.5 for the α-domain, 12.7, 12.4, and 12.0 for the β-domain, and 13.3, 13.1, 12.7, 12.4, 12.0, 11.3, and 10.8 for the full MT protein, as shown in Figure 5. The key features (a′–e′) in the experimental data are modeled in the simulation (a–e, respectively).

Figure 6. continued

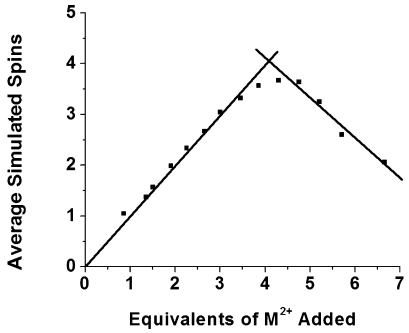

Figure 7. Simulated EPR spectral data based upon metalation of apo-$\beta\alpha$-rhMT with Zn^{2+} forming first the nonclustered Zn_5-$\beta\alpha$-rhMT followed by cluster formation in the two domains up to Zn_7-$\beta\alpha$-rhMT. The simulated average number of spins was calculated assuming Zn^{2+} has the same spin as Co^{2+}. The exact metalation state (noting the onset of clusters) was obtained from analysis of the data in Figure 4. The method for determining the average number of simulated spins is described in the text.

Relevance of Previously Published Co^{2+} EPR Data. Co^{2+}, with its rich spectroscopic properties and characteristic tetrahedral coordination with thiols, has been extensively used to mimic Zn^{2+} binding to MT. Uniquely, the EPR intensity of Co^{2+} is directly related to the number of Co^{2+} atoms present in MT and the number of nonclustered Co^{2+} centers. In work by Vasak and Kagi, metalation of MT with Co^{2+} was monitored using EPR spectroscopy.[S4] Analysis of the data when plotted as a function of added Co^{2+} showed an increase in the number of free spins until 4 molar equiv had been added, after which antiferromagnetic coupling led to a decrease in the signal intensity approaching zero after the addition of 7 equiv. These data were interpreted as cluster formation taking place after four metal ions had been added.

We have simulated the EPR experiment using our Zn data that show the exact distribution of metals in nonclustered sites (up to five Zn^{2+} ions bound) and clustered sites (six and seven Zn^{2+} ions bound). We assigned a fictitious spin to the nonbridging Zn^{2+} ions as a Co^{2+} mimic while canceling the spins when clustering occurred (Figure 7). We used the following rules to simulate the predicted, fictitious magnetic moment: Zn_1-rhMT through Zn_5-rhMT are formed without any bridging interactions and consequently increase the magnitude of the EPR signal; the formation of Zn_6- and Zn_7-rhMT requires four and eight bridging interactions, respectively, and consequently decreases the magnitude of the signal due to antiferromagnetic coupling. The simulated EPR data (Figure 7) closely resemble the original Co^{2+} data with a maximum at approximately 4.5 (we show the average number of spins rather than the calculated g factor). While we would intuitively predict five M^{2+} ions are necessary for maximal intensity in our model, the noncooperative nature of metalation requires that some M_6-rhMT exist at this metal loading. In the Co^{2+} titration, this species would greatly decrease the signal intensity. We suggest that the high degree of similarity between our modeled data, based upon ESI-MS speciation data, and the

dx.doi.org/10.1021/bi400021b | Biochemistry 2013, 52, 2461–2471

original Co^{2+} data supports our proposal that clustering does not occur until the sixth metal ion is added and that Zn_5-rhMT is a single-domain species that does not involve bridging Cys.

Molecular Modeling of a Potential Metalation Pathway. Figure 8 shows the results of a series of molecular dynamics calculations that predict plausible structural changes that could occur during the progressive metalation of apo-$\beta\alpha$-rhMT by Zn^{2+} to the intermediate Zn_5-$\beta\alpha$-rhMT, and finally Zn_7-$\beta\alpha$-rhMT. The minimized (5000 ps) apo-$\beta\alpha$-rhMT structure (A) resembles that reported by Rigby et al.[50,51,55] showing a globular fold with the free cysteinyl thiols aligned on the surface. Tetrahedral Zn^{2+} coordination by terminal Cys was arranged for the first five Zn^{2+} ions forming a single 5-Zn-20-S_{Cys} binding domain. We should note that the Zn_5- and Zn_6-$\beta\alpha$-rhMT species presented (Figure 8B,C) are of a qualitative nature. Without definitive structural information, alternative connectivities may be possible. Despite the lack of cluster formation in Zn_5-$\beta\alpha$-rhMT, the overall three-dimensional structure of the protein resembles that of the fully metalated Zn_7-protein. Even when there are no bridging Cys residues present, the Zn_5-$\beta\alpha$-rhMT model shows the two Zn^{2+} ions in the β-domain Cys [i.e., within the fragment of residues 1−36 (Figure 8)] and the three Zn^{2+} ions in the α-domain Cys (i.e., within the fragment of residues 37−74) are spatially close to one another. This likely facilitates cluster formation upon further metalation to the traditional two-domain Zn_7-$\beta\alpha$-rhMT (Figure 8 D).

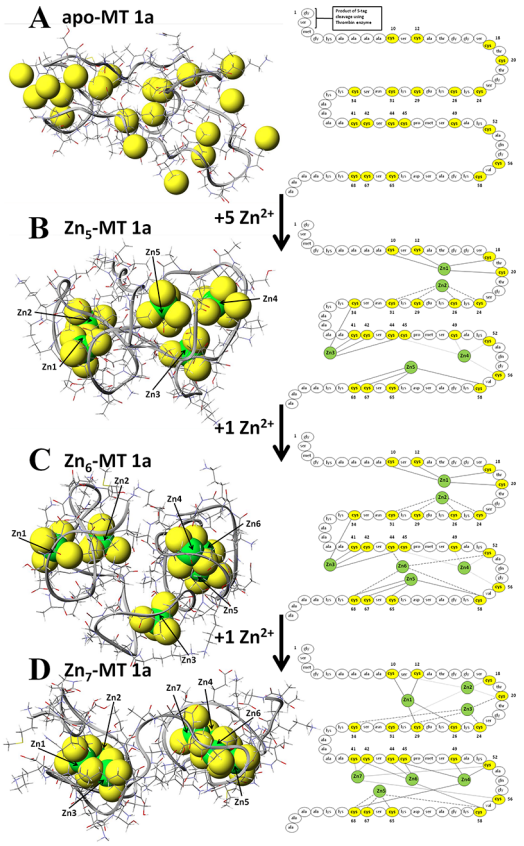

Figure 8. Molecular models of possible structures formed from apo-rhMT by the addition of Zn^{2+} (left) and the amino acid sequence of $\beta\alpha$-rhMT showing connectivities of the increasing numbers of Zn^{2+} ions (right). Ribbons show the backbone, with Zn^{2+} represented as green spheres and sulfur atoms as yellow spheres. The N-terminal β-domain is located at the left and the C-terminal α-domain at the right. (A) Metal-free, apo-$\beta\alpha$-rhMT (structure first reported by Rigby et al.[55]), (B) Single-domain Zn_5-$\beta\alpha$-rhMT (structure created by assigning four terminal Cys residues to each Zn^{2+}). (C) One possible structure for Zn_6-$\beta\alpha$-rhMT based on Cys known to bridge in the saturated two-domain structure. (D) Formation of Zn_7-$\beta\alpha$-rhMT with rearrangement of bound metals and addition of Zn7. Structures were calculated using a locally modified force field with the Scigress MM3/MD methods.[45] Minimization of the structures was conducted for 5000 ps at 300 K. The conformer with the lowest energy is presented above. The initial structure of Cd_7-$\beta\alpha$-rhMT 1a, modified for all subsequent structures, was provided by Chan et al.[43]

SUMMARY AND CONCLUSIONS

We have shown that with the onset of cluster formation (as defined by the use of bridging vs terminal cysteine thiolate groups) there is a significant decrease in the Zn binding affinity of MT and its domains. This is caused by the decrease in K_F associated with cluster formation.

Previous experimental metalation studies of binding of Zn^{2+} to $\beta\alpha$-rhMT have been analyzed mechanistically in terms of cooperative and noncooperative models. Only the noncooperative mechanism simulated the experimental data.[48] Modeling of the ESI-MS data reported herein allowed us to conclude that the decreasing K_F values of a noncooperative metalation mechanism led to formation of a stable Zn_5-$\beta\alpha$-rhMT species, without bridging interactions. This is mechanistically a key member of the metalation pathway from apo-rhMT to the saturated Zn_7-rhMT.

The sixth and seventh Zn^{2+} ions act as a buffer with K_F values lower than those of the five structural Zn^{2+} ions, allowing MT to donate and acquire Zn^{2+} without oxidizing any Cys residues in the protein. In the cellular environment, this positions Zn-MT as the main Zn^{2+} sink, buffering intracellular Zn^{2+} levels between the detection limits of Zn sensors, such as ZiaR[52] and Zur,[53] within the Zn sequestration equilibrium.

Our recently published study of the supermetalation of MT 1a, where addition of an eighth Cd^{2+} ion leads to the coalescence of the two domains to form one "superdomain",[44] suggests a view of the metalation properties of MT fundamentally altered from that of maintaining two domains, regardless of metal depletion, to a new structural characterization of MT, where MT exists as a flexible, single-domain protein during initial metalation (<5 equiv) and metalation in excess of traditional levels (>7 equiv).

ASSOCIATED CONTENT

Supporting Information

Raw ESI-MS data that complement the deconvoluted spectra in Figures 2 and 5 (Figures S1 and S2, respectively). Figure S1 shows the charge states recorded for the competitive titration of Zn^{2+} with the two isolated domains. Figure S2 shows the charge states for the competitive titration of Zn^{2+} with the two domains and full MT protein. This material is available free of charge via the Internet at http://pubs.acs.org.

AUTHOR INFORMATION

Corresponding Author

*Department of Chemistry, The University of Western Ontario, London, Canada N6A 5B7. Phone: (519) 661-3821. E-mail: martin.stillman@uwo.ca.

Author Contributions

K.L.S. and D.E.K.S. contributed equally to this work.

Funding

We thank NSERC of Canada for financial support through a Discovery Grant and a Research Tools and Instruments Grant (to M.J.S.) and an Alexander Graham Bell Canada Graduate Scholarship (to D.E.K.S.). We also thank The University of Western Ontario for an Academic Development Fund Grant.

Notes

The authors declare no competing financial interest.

■ ACKNOWLEDGMENTS

We thank Mr. Doug Hairsine for technical assistance.

■ ABBREVIATIONS

MT, metallothionein; β-rhMT 1a, recombinantly prepared β-domain of human metallothionein isoform 1a; α-rhMT 1a, recombinantly prepared α-domain of human metallothionein isoform 1a; $\beta\alpha$-rhMT 1a, recombinantly prepared human metallothionein isoform 1a; ESI, electrospray ionization; MS, mass spectrometry; EPR, electron paramagnetic resonance; K_F, formation constant.

■ REFERENCES

(1) Vallee, B. L., and Falchuk, K. H. (1993) The biochemical basis of zinc physiology. *Physiol. Rev. 73*, 79−118.
(2) Prasad, A. S. (1995) Zinc: An overview. *Nutrition 11*, 93−99.
(3) Beyersmann, D., and Haase, H. (2001) Functions of zinc in signaling, proliferation and differentiation of mammalian cells. *BioMetals 14*, 331−341.
(4) Eide, D. J. (2004) The SLC39 family of metal ion transporters. *Pfluegers Arch. 447*, 796−800.
(5) Yamasaki, S., Hasegawa, A., Hojyo, S., Ohashi, W., Fukada, T., Nishida, K., and Hirano, T. (2012) A novel nole of the L-type calcium channel α(1D) subunit as a gatekeeper for intracellular zinc signaling: Zinc wave. *PLoS One 7*, No. e39654.
(6) Waldron, K. J., and Robinson, N. J. (2009) How do bacterial cells ensure that metalloproteins get the correct metal? *Nat. Rev. 6*, 25.
(7) Lee, D. K., Geiser, J., Dufner-Beattie, J., and Andrews, G. K. (2003) Pancreatic metallothionein-l may play a role in zinc homeostasis during maternal dietary zinc deficiency in mice. *J. Nutr. 133*, 45−50.
(8) Lichtlen, P., and Schaffner, W. (2001) Putting its fingers on stressful situations: The heavy metal-regulatory transcription factor MTF-1. *BioEssays 23*, 1010−1017.
(9) Fukada, T., Yamasaki, S., Nishida, K., Murakami, M., and Hirano, T. (2011) Zinc homeostasis and signaling in health and diseases: Zinc signaling. *J. Biol. Inorg. Chem. 16*, 1123−1134.
(10) Ugarte, M., and Osborne, N. N. (2001) Zinc in the retina. *Prog. Neurobiol. 64*, 219−249.
(11) Robinson, N. J. (2008) A bacterial copper metallothionein. *Nat. Chem. Biol. 4*, 582−583.
(12) Tucker, S. L., Thornton, C. R., Tasker, K., Jacob, C., Giles, G., Egan, M., and Talbot, N. J. (2004) A fungal metallothionein is required for pathogenicity of *Magnaporthe grisea*. *Plant Cell 16*, 1575−1588.
(13) King, G., Price, D., Rice, W., and Joshi, J. G. (1982) Interrelationship of zinc, ferritin, metallothionein and small molecular-weight components in plants and animals. *Fed. Proc. 41*, 641.
(14) Feng, W., Cai, J., Pierce, W. M., Franklin, R. B., Maret, W., Benz, F. W., and Kang, Y. J. (2005) Metallothionein transfers zinc to mitochondrial aconitase through a direct interaction in mouse hearts. *Biochem. Biophys. Res. Commun. 332*, 853−858.
(15) Mason, A. Z., Perico, N., Moeller, R., Thrippleton, K., Potter, T., and Lloyd, D. (2004) Metal donation and apo-metalloenzyme activation by stable isotopically labeled metallothionein. *Mar. Environ. Res. 58*, 371−375.
(16) Li, T.-Y., Kraker, A. J., Shaw, C. F., III, and Petering, D. H. (1980) Ligand substitution reactions of metallothioneins with EDTA and apo-carbonic anhydrase. *Proc. Natl. Acad. Sci. U.S.A. 77*, 6334−6338.
(17) Maret, W., Larsen, K. S., and Vallee, B. L. (1997) Coordination dynamics of biological zinc "clusters" in metallothioneins and in the DNA-binding domain of the transcription factor Gal4. *Proc. Natl. Acad. Sci. U.S.A. 94*, 2233−2237.
(18) Zeng, J., Heuchel, R., Schaffner, W., and Kagi, J. H. R. (1991) Thionein (apometallothionein) can modulate DNA binding and transcription activation by zinc finger containing factor Sp1. *FEBS Lett. 279*, 310−312.
(19) Zaia, J., Fabris, D., Wei, D., Karpel, R. L., and Fenselau, C. (1998) Monitoring metal ion flux in reactions of metallothionein and drug-modified metallothionein by electrospray mass spectrometry. *Protein Sci. 7*, 2398−2404.
(20) Leszczyszyn, O. I., and Blindauer, C. A. (2010) Zinc transfer from the embryo-specific metallothionien E_c from wheat: A case study. *Phys. Chem. Chem. Phys. 12*, 13408−13418.
(21) Leszczyszyn, O. I., Evans, C. D., Keiper, S. E., Warren, G. Z. L., and Blindauer, C. A. (2007) Differential reactivity of individual zinc ions in clusters from bacterial metallothioneins. *Inorg. Chim. Acta 360*, 3−13.
(22) Ngu, T. T., and Stillman, M. J. (2006) Arsenic binding to human metallothionein. *J. Am. Chem. Soc. 128*, 12473−12483.
(23) Nielson, K. B., Atkin, C. L., and Winge, D. R. (1985) Distinct metal-binding configurations in metallothionein. *J. Biol. Chem. 260*, 5342−5350.
(24) Lu, W., and Stillman, M. J. (1993) Mercury-thiolate clusters in metallothionein. Analysis of circular dichroism spectra of complexes formed between α-metallothionein, apometallothionein, zinc metallothionein, and cadmium metallothionein and Hg^{2+}. *J. Am. Chem. Soc. 115*, 3291−3299.
(25) Robbins, A. H., McRee, D. E., Williamson, M., Collett, S. A., Xuong, N. H., Furey, W. F., Wang, B. C., and Stout, C. D. (1991) Refined crystal structure of Cd, Zn metallothionein at 2.0 Å resolution. *J. Mol. Biol. 221*, 1269−1293.
(26) Messerle, B. A., Schaffer, A., Vasak, M., Kagi, J. H. R., and Wuthrich, K. (1992) Comparison of the solution conformations of human $[Zn_7]$-metallothionein-2 and $[Cd_7]$-metallothionein-2 using nuclear magnetic resonance spectroscopy. *J. Mol. Biol. 225*, 433−443.
(27) Messerle, B. A., Schaffer, A., Vasak, M., Kagi, J. H. R., and Wuthrich, K. (1990) Three-dimensional structure of human $[^{113}Cd_7]$-metallothionein-2 in solution determined by nuclear magnetic resonance spectroscopy. *J. Mol. Biol. 214*, 765−779.
(28) Salgado, M. T., and Stillman, M. J. (2004) Cu^+ distribution in metallothionein fragments. *Biochem. Biophys. Res. Commun. 318*, 73−80.
(29) Ngu, T. T., Easton, A., and Stillman, M. J. (2008) Kinetic analysis of arsenic-metalation of human metallothionein: Significance of the two-domain structure. *J. Am. Chem. Soc. 130*, 17016−17028.
(30) Ngu, T. T., Lee, J. A., Rushton, M. K., and Stillman, M. J. (2009) Arsenic metalation of seaweed *Fucus vesiculosus* metallothionein: The importance of the interdomain linker in metallothionein. *Biochemistry 48*, 8806−8816.
(31) Sutherland, D. E. K., Summers, K. L., and Stillman, M. J. (2012) Noncooperative metalation of metallothionein 1a and its isolated domains. *Biochemistry 51*, 6690.
(32) Rigby-Duncan, K. E., and Stillman, M. J. (2007) Evidence for noncooperative metal binding to the α domain of human metallothionein. *FEBS J. 274*, 2253−2261.
(33) Sutherland, D. E. K., and Stillman, M. J. (2008) Noncooperative cadmium(II) binding to human metallothionein 1a. *Biochem. Biophys. Res. Commun. 372*, 840−844.
(34) Palumaa, P., Eriste, E., Njunkova, O., Pokras, L., Jornvall, H., and Sillard, R. (2002) Brain-specific metallothinein-3 has higher metal-binding capacity than ubiquitous metallothioneins and binds metals noncooperatively. *Biochemistry 41*, 6158−6163.

(35) Ngu, T. T., Krecisz, S., and Stillman, M. J. (2010) Bismuth binding studies to the human metallothionein using electrospray mass spectrometry. *Biochem. Biophys. Res. Commun. 396*, 206−212.
(36) Ngu, T. T., Lee, J. A., Pinter, T. B. J., and Stillman, M. J. (2010) Arsenic-metalation of triple-domain human metallothioneins: Support for the evolutionary advantage and interdomain metalation of multiple-metal-binding domains. *J. Inorg. Biochem. 104*, 232−244.
(37) Namdarghanbari, M. A., Meeusen, J., Bachowski, G., Giebel, N., Johnson, J., and Petering, D. H. (2010) Reaction of the zinc sensor FluoZin-3 with Zn(7)-metallothionein: Inquiry into the existance of a proposed weak binding site. *J. Inorg. Biochem. 104*, 224−231.
(38) Krezel, A., and Maret, W. (2007) Dual nanomolar and picomolar Zn(II) binding properties of metallothionein. *J. Am. Chem. Soc. 129*, 10911−10921.
(39) Summers, K. L., Mahrok, A. K., Dryden, M. D. M., and Stillman, M. J. (2012) Structural properties of metal-free apometallothioneins. *Biochem. Biophys. Res. Commun. 425*, 485−492.
(40) Stillman, M. J. (1995) Metallothioneins. *Coord. Chem. Rev. 144*, 461−511.
(41) Sutherland, D. E. K., and Stillman, M. J. (2011) The "magic numbers" of metallothionein. *Metallomics 3*, 444−463.
(42) Kang, Y. J. (2006) Metallothionein redox cycle and function. *Exp. Biol. Med. 231*, 1459−1467.
(43) Chan, J., Huang, Z., Watt, I., Kille, P., and Stillman, M. J. (2007) Characterization of the conformational changes in recombinant human metallothioneins using ESI-MS and molecular modeling. *Can. J. Chem. 85*, 898−912.
(44) Sutherland, D. E. K., Willans, M. J., and Stillman, M. J. (2012) Single domain metallothioneins: Supermetalation of human MT 1a. *J. Am. Chem. Soc. 134*, 3290−3299.
(45) Chan, J., Merrifield, M. E., Soldatov, A. V., and Stillman, M. J. (2005) XAFS spectral analysis of the cadmium coordination geometry in cadmium thiolate clusters in metallothionein. *Inorg. Chem. 44*, 4923−4933.
(46) Chan, J., Huang, Z., Merrifield, M. E., Salgado, M. T., and Stillman, M. J. (2002) Studies of metal binding reactions in metallothionein by spectroscopic, molecular biology, and molecular modeling techniques. *Coord. Chem. Rev. 233−234*, 319−339.
(47) Salgado, M. T., Bacher, K. L., and Stillman, M. J. (2007) Probing structural changes in the α and β domains of copper- and silver-substituted metallothionein by emission spectroscopy and electrospray ionization mass spectrometry. *J. Biol. Inorg. Chem. 12*, 294−312.
(48) Sutherland, D. E. K., Summers, K. L., and Stillman, M. J. (2012) Modeling the Zn^{2+} and Cd^{2+} metalation mechanism in mammalian metallothionein 1a. *Biochem. Biophys. Res. Commun. 426*, 601−607.
(49) Duncan, K. E. R., Ngu, T. T., Chan, J., Salgado, M. T., Merrifield, M. E., and Stillman, M. J. (2006) Peptide folding, metal-binding mechanisms, and binding site structures in metallothioneins. *Exp. Biol. Med. 231*, 1488−1499.
(50) Rigby, K. E., Chan, J., Mackie, J., and Stillman, M. J. (2006) Molecular dynamics study on the folding and metallation of the individual domains of metallothionein. *Proteins: Struct., Funct., Bioinf. 62*, 159−172.
(51) Duncan, K. E. R., and Stillman, M. J. (2006) Metal-dependent protein folding: Metallation of metallothionein. *J. Inorg. Biochem. 100*, 2101−2107.
(52) VanZile, M. L., Cosper, N. J., Scott, R. A., and Giedroc, D. P. (2000) The zinc metalloregulatory protein *Synechococcus* PCC7942 SmtB binds a single zinc ion per monomer with high affinity in a tetrahedral coordination geometry. *Biochemistry 39*, 11818−11829.
(53) Ma, Z., Gabriel, S. E., and Helmann, J. D. (2011) Sequential binding and sensing of Zn(II) by *Bacillus subtilis* Zur. *Nucleic Acids Res. 39*, 9130−9138.
(54) Vasak, M., and Kagi, J. H. R. (1981) Metal thiolate clusters in cobalt(II)-metallothionein. *Proc. Natl. Acad. Sci. U.S.A. 78*, 6709−6713.
(55) Rigby, K. E., and Stillman, M. J. (2004) Structural studies of metal-free metallothionein. *Biochem. Biophys. Res. Commun. 325*, 1271−1278.